Sciencexpress Report

Exposed Water Ice Discovered Near the South Pole of Mars

Timothy N. Titus,[1] Hugh H. Kieffer,[1] Phillip R. Christensen[2]

[1]Branch of Astrogeology, U.S. Geological Survey, 2255 North Gemini Drive, Flagstaff, AZ 86001, USA. [2]Department of Geological Sciences, Arizona State University, Tempe, AZ 85287, USA.

The Mars Odyssey Thermal Emission Imaging System (THEMIS) has discovered water ice exposed near the edge of Mars' southern perennial polar cap. The surface H_2O ice was first observed by THEMIS as a region that was cooler than expected for dry soil at this latitude during the summer season. Diurnal and seasonal temperature trends derived from Mars Global Surveyor (MGS) Thermal Emission Spectrometer (TES) observations indicate that there is water ice at the surface. Viking observations, and the few other relevant THEMIS observations, indicate that surface water ice may be widespread around and under the perennial CO_2 cap.

Determining the abundance and distribution of surface and near-surface H_2O ice is fundamental for both understanding the hydrological cycle and for the future exploration of Mars. Water ice, at or near the surface, is available for surface interactions and exchange with the atmosphere. Water ice that is buried a meter or more has a time constant for interaction with the atmosphere longer than a martian year, and is thus relatively inactive (*1*). In addition, H_2O ice that is in the top few centimeters of soil will probably be accessible to future robotic probes, and ultimately, human exploration. Apart from the residual north polar cap, exposed H_2O ice may be limited to certain types of topographic features having spatial scales of the order of hundreds of meters, not hundreds of kilometers.

The martian seasonal caps had been erroneously identified as H_2O (*2*) before modeling (*3*) indicated that CO_2 provided an excellent fit to the seasonal progression of the cap. The north polar perennial cap is water ice based on observations of late summer surface temperatures (*4*) and associated atmospheric water vapor abundances (*5*). In late summer in the south polar area, when the seasonal CO_2 has retreated to its annual minimum extent, the only exposed volatile material to be identified was CO_2 (*6, 7*). Annual temperature observations of the north polar region had indicated the presence of ground H_2O ice (*8*) but no water ice has been identified in the southern hemisphere, although thermal modeling has indicated water ice would be stable in the subsurface (*1*). The mean annual atmospheric H_2O saturation temperature is higher than the mean annual surface temperature in the south polar region, indicating that H_2O accumulation is inevitable. The extensive layered deposits in both polar regions have commonly been assumed to contain significant H_2O ice (*9–11*). Viking thermal observations has indicated the difficulty of thermally detecting water ice below a few cm of dust, and no positive indication of water ice has previously been made in the southern hemisphere (*12*). Modeling of the potential flow of dust-ice mixtures has suggested that the polar layered deposits must contain <40% or >90% water ice by volume (*13*). The Mars Odyssey Gamma Ray Spectrometer (GRS) has measured an abundance of hydrogen over the circum-polar region indicating probable saturation of the subsurface with water ice in the first meter (*14, 15*).

THEMIS thermal and visible observations near 85.5°S, 10°E at L_s = 334° (late southern summer) show several distinct uniform regions. There is an elongated region (Fig. 1, unit I) with a uniform temperature of 185 ± 3 K and Lambertian albedo of 0.30 (*16*). Unit I is noticeably cooler than an adjacent area with a temperature of 198 ± 2 K (Fig. 1, unit S) and a Lambertian albedo of 0.23, which is similar to much of the martian soil surface. While brighter regions are generally cooler than adjacent darker regions, the relative brightness of unit I is not sufficient to explain its depressed temperature. The MOLA topography of this area indicates a weak, broad ridge, roughly along the I/S boundary; the slopes on both sides are ~0.5°. Immediately to the south, adjacent to unit I, is a narrow strip of seasonal CO_2 (*17*). To the south of this is a relatively warm equator-facing 6º slope of layered terrain (unit D). At the top of this slope is a plateau covered by perennial CO_2 (unit C) (*18*).

Seasonal and diurnal temperature trends are needed to constrain the thermal properties of these surface units, and thus help constrain probable composition. We use TES bolometer observations (*19*), collected over two consecutive martian years, to determine the seasonal and diurnal thermal trends of the identified units. The repeatability of the late summer temperature trends between these two years, one a relatively clear year and the other year dusty in the spring (L_s ~ 200º-240º), suggests a process that is stable between martian years, regardless of the annual martian climate. This entire region (Fig. 1) is annually covered by the seasonal CO_2 cap (*20*). The observed temperatures for both units S and I rise from CO_2 ice values over about 20 sols (*21*), indicating a variation in the date of final CO_2 disappearance below the spatial resolution of TES. The CO_2 first disappears from the unit S terrain at L_s = 290º (early summer). Initially, the temperature rises rapidly to approximately 200 K, without significant diurnal variation. At L_s = 305º, the daytime temperatures suddenly jump 20º while the nighttime temperatures remained near 200 K. At L_s = 310º, the CO_2 finally disappeared from unit I, resulting in a slow rise of the temperature until it reaches a peak of 205 K around L_s = 318º. Minimal diurnal variation was observed, suggesting high thermal inertia. After L_s = 318º, temperatures slowly drop with decreasing insolation to the values observed by THEMIS.

Thermal models were computed for the location and elevation of units I and S (*22, 23*). Unit I is best fit by a homogeneous material with thermal inertia of about 1600-2000 $Jm^{-2}\ K^{-1}s^{-1/2}$; the observed diurnal variation is somewhat greater than in the models, possibly due to some dust grains on the surface that are thermally isolated from the high-inertia material. In addition to the possible effects of surface dust grains, some of the scatter in brightness temperatures can be attributed to subpixel mixing with adjacent units (*24*). The derived thermal inertia is similar to the value for water ice. The geologic setting of high elevation surrounded by thick polar layered deposits and the rarity of thermal inertia above 800 $Jm^{-2} K^{-1}s^{-1/2}$ elsewhere on the planet (*25*) make it unlikely that the high inertia is due to exposed rock (*26*).

Before L_s = 300°, unit S data is best fit by a homogeneous material similar to unit I. At L_s = 300°, the diurnal thermal behavior of unit S suddenly changes, suggestive of a change from high thermal inertia to lower thermal inertia. At this point, unit S data are not fit well by any model of homogeneous materials, however the data can be fit by a 7-mm-thick layer of material with thermal inertia of 50 $Jm^{-2} K^{-1}s^{-1/2}$ on top of a substrate with thermal inertia of 2000 $Jm^{-2} K^{-1}s^{-1/2}$ (Fig. 2). A 2-mm-layer of low-inertia material over a substrate with thermal inertia of 1200 $Jm^{-2} K^{-1}s^{-1/2}$ fits nearly as well. The thermal observations indicate that unit S is laterally uniform and hint that the thermal inertia of the surface layer decreases through the summer (*27*).

As CO_2 sublimes in the spring, the seasonal frost deposit remains at 145 K, and H_2O in that frost (*28*) will remain solid. If the H_2O grains, probably containing a core of dust, are heavy enough that they are not raised by the CO_2 sublimation wind (*29*), they will accumulate as a lag deposit until the crocus date [the date of final disappearance of solid CO_2 (*30*)]. The surface temperatures will rise to 190 K in a few days at most, at which temperature the H_2O will go into the gas phase and be mobile. Some H_2O will escape into the atmosphere, and some may diffuse into the cool soil below. This annual H_2O could escape in the late summer as the surficial dust layer becomes too warm, thus closing the annual cycle. We suspect that the stable solution at this latitude will be a low inertia surface layer that “hydrates” and “desiccates” annually, over a substrate of high-inertia ground water ice, similar to the calculations of Mellon.

The contact between units I and S shown in Fig. 1 is sharp and nearly linear, and has been that way for decades. Published ground-ice models (*31*) do not yield abrupt lateral changes of stable conditions, so we feel that some unidentified process with positive feedback must be responsible for this sharp contact, maintaining two stable configurations in a virtually uniform environment. Because conditions are similar for all these units when they are CO_2 covered, this process must be active in the late summer, when at least some of the units are bare of the seasonal CO_2 ice.

Unit I is darker than the H_2O ice in the north polar cap. The low albedo of unit I is probably responsible for it not having previously been identified as H_2O ice. A small-to-modest fraction of dust can cause water ice albedos in this range (*32*).

TES observations suggest that the existence of units I and S have been stable since MGS achieved mapping orbit around Mars. TES albedo measurements also suggest that the observed thermal boundary that is observed by THEMIS should also be an albedo boundary. Indeed, wide angle Mars Orbiter Camera (MOC) imaging has verified that the contact between units S and I is an albedo boundary as well as a thermal boundary. Viking observations from a quarter of a century ago reveal the exact same albedo boundary as seen in MOC imaging (Fig. 3), suggesting that these two units have been stable over several decades.

Herkenhoff (*33*) used Viking color data to identify a unit in this region of intermediate albedo and color that he interpreted as being soil partially defrosted of CO_2 ice; designated Af. Our thermally identified unit I spatially corresponds to unit Af. Preliminary analysis of TES thermal seasonal trends, similar to the analysis conducted for unit I (Fig. 2) cannot rule out the possibility that unit I and unit Af are identical. If this is true, exposed water ice at the surface may be quite wide spread. A few other THEMIS thermal images of the late summer southern cap edge show further evidence of intermediate surface temperatures, further suggesting that areas of exposed water ice between 1 to 10 km wide may be common along the perennial cap edge. Water vapor observations of the south-polar summer (*34–36*) suggest that the amount is variable from year to year. However, the crocus dates for the units I and S are not distinguishable different between the 2000 and 2002 TES observations. The inter-annual water vapor variability may be a result of local surface variations of unit Af outside of the THEMIS scene.

Various indirect (*34, 37*) and direct (*38*) observations of the south polar region have suggested that the perennial CO_2 cap is not constant and may periodically disappear altogether. Because of the long-term stability of H_2O at current south-polar temperatures, and because solid CO_2 must be at the surface (*39*), it is possible that the water ice layer extends under the current CO_2 perennial cap.

References and Notes

1. Farmer and Doms first computed the basic distribution of ground ice on the basis of sub-surface temperatures being below the current mean atmospheric water vapor saturation temperature. (*40*). Zent, Fanale, Savail and Postawko (*41*) included treatment of sub-surface gas diffusion and adsorption over obliquity cycles. Paige (*42*) found that the extent of stable ice was increased by consideration of likely layered soils. In a series of papers, Mellon has modeled the probable distribution (latitude, longitude, depth and time) of ground ice over several million years (*43–45*).
2. V. I. Moroz, *Soviet Astron.* **8**, 273 (1964).
3. R. B. Leighton, B. C. Murray, *Science* **153**, 136 (1966).
4. H. H. Kieffer *et al.*, *J. Geophys. Res.* **194**, 1341 (1976).
5. C. B. Farmer, D. W. Davies, D. D. LaPorte, *Science* **194**, 1339 (1976).
6. H. H. Kieffer, *J. Geophys. Res.* **84**, 8263 (1979).
7. D. A. Paige, K. E. Herkenhoff, B. C. Murray, *J. Geophys. Res.* **95**, 1913 (1990).
8. D. A. Paige, J. E. Bachman, K. D. Keegan, *J. Geophys. Res.* **99**, 25959 (1994).
9. J. A. Cutts, *J. Geophys. Res.* **78**, 4231 (1973).
10. K. E. Herkenhoff, B. C. Murray, *J. Geophys. Res.* **95**, 1343 (1990).
11. P. Thomas, S. Squyres, K. Herkenhoff, A. Howard, B. Murray, in *Mars*, H. Kieffer *et al.*, Eds. (Univ. of Arizona Press, Tucson, AZ, 1992), chap. 23.
12. D. A. Paige, K. D. Keegan, *J. Geophys. Res.* **99**, 25993 (1994).
13. M. D. Hofstadter, B. C. Murray, *Icarus* **84**, 352 (1990).
14. W. V. Boynton *et al.*, *Science* **297**, 81 (2002).
15. Reviews of martian conditions are: Polar caps:(*46*), Water in the atmosphere: (*47*), Annual polar caps: (*48*).
16. TES albedo measurements were used because the THEMIS VIS images are not currently radiometrically calibrated.
17. The strip of seasonal CO_2 that lies between unit I and unit D narrows in size as summer progresses.

18. The default calibration yielded brightness temperatures for unit C below the saturation temperature of CO_2 at the surface elevation. The radiance levels for the entire THEMIS strip were adjusted to bring the brightness temperature of unit C to 144 K, as expected from extensive TES observations.
19. Bolometer observations were used instead of the spectrometer observations because of better spatial and temporal coverage.
20. MOC imaging of this region during early spring showed only the "D" unit as not completely covered by CO_2.
21. A sol is one full martian day, 24.6 hours.
22. The properties of pure solid H_2O at 165 K are: thermal conductivity k = 3.42 J/(m s K), density ρ = 928 kg/m^3, specific heat C_p = 1310 J/(kg K), yielding a thermal inertia $(k\rho C_p)^{1/2} = 2044$ Jm^{-2} K^{-1}s$^{-1/2}$.
23. The models solve the subsurface thermal diffusion equation with a boundary condition of insolation and a one-layer atmosphere using the Delta-Eddington radiative approximation. A typical Martian dust opacity of 0.2 is used, with CO_2 frost condensation if the temperature falls below the saturation point for the current local atmospheric pressure. The Viking lander seasonal pressure variation is used (*49*). Models were run for 4 years to attain annual convergence, adjusting the solid CO_2 budget to disappear at the observed date for each area, then for another 80 martian days (sol) with 1-sol spacing.
24. A nominal TES footprint is either 3 km × 5 km or 3 km × 9 km, depending on whether TES is operating in 10 cm^{-1} or 5 cm^{-1} mode, respectively.
25. M. T. Mellon, B. M. Jakosky, H. H. Kieffer, P. R. Christensen, *Icarus* **148**, 437 (2000).
26. Typical thermal inerta for dust and rock are 50 Jm^{-2} K^{-1}s$^{-1/2}$, 1260 Jm^{-2} K^{-1}s$^{-1/2}$, respectively.
27. At the observed maximum temperature (200K at L_s = 315°), the I unit will be subliming into the atmosphere, and this will somewhat suppress the temperatures. Although the sublimation rate is difficult to constrain without knowledge of the lowest boundary layer conditions, an estimate can be made by assuming that the column water vapor typical of late summer conditions, about 10 precipital micrometers (*35, 36*) is replenished every martian day. This corresponds to a sublimation power of 0.3 W/m^2, or about 0.2% of the average absorbed solar flux; the surface temperature is lowered by less than 0.2K.
28. H_2O grains in the atmosphere probably nucleate on dust grains. H_2O and dust probably accumulate with the south polar seasonal frost; both with mixing ratios to CO_2 of about 10^{-4} (*34*).
29. See Fig. 17 in (*30*).
30. H. Kieffer, T. Titus, K. Mullins, P. Christensen, *J. Geophys. Res.* **105**, 9653 (2000).
31. See Mellon, 1993 (*43*), 1995 (*44*), and 1997 (*45*), for a detailed discussion.
32. Based on modeling of the albedo of dust-ice mixtures for the north polar cap, the increment of albedo from 0.23 to 0.30 for the S-I transition indicates that $f\,(r_H/r_d)^3 \sim 3$, where r_H is the ice grain radius, r_d the dust grain radius, and f the dust fraction. Thus, assuming the dust is captured atmospheric dust (~2 micron radius), dust fractions of 0.1 and 0.0001 would imply ice grain radii of 8 to 80 micrometers.
33. K. E. Herkenhoff, *USGS Misc. Inv. Series Map Series I-2686* (2001).
34. E. S. Barker, R. A. Schorn, A. Woszczyk, R. G. Tull, S. J. Little, *Science* **170**, 1308 (1970).
35. B. Jakosky, J. Farmer, *J. Geophys. Res.* **87**, 2999 (1982).
36. M. D. Smith, J. L. Bandfield, M. I. Richardson, P. R. Christensen, paper presented at the annual meeting of the Division of Planetary Scientists, Birmingham, AL, 6–11 October 2002.
37. B. M. Jakosky, R. M. Haberle, *J. Geophys. Res.* **95**, 1359 (1990).
38. M. C. Malin, M. A. Caplinger, S. D. Davis, *Science* **294**, 2146 (2001).
39. CO_2 would quickly sublime if it were buried under a warmer material, and nothing with connection to the atmosphere can be colder than solid CO_2.
40. C. B. Farmer, P. E. Doms, *J. Geophys. Res.* **84**, 2881 (1979).
41. A. P. Zent, F. P. Fanale, J. R. Salvail, S. E. Postawko, *Icarus* **67**, 19 (1986).
42. D. A. Paige, *Nature* **356**, 43 (1992).
43. M. T. Mellon, B. M. Jakosky, *J. Geophys. Res.* **98**, 3345 (1993).
44. ———, *J. Geophys. Res.* **100**, 11781 (1995).
45. ———, S. W. Postawko, *J. Geophys. Res.* **102**, 19357 (1997).
46. F. Forget, in *Solar System Ices*, B. Schmidtt *et al.*, Eds. (Kluwer Academic, Dordrecht, Netherlands, 1998), pp. 447–510.
47. B. M. Jakosky, R. M. Haberle, in *Mars*, H. Kieffer *et al.*, Eds. (Univ. of Arizona Press, Tucson, AZ, 1992), chap. 28.
48. P. B. James, H. H. Kieffer, D. A. Paige, in *Mars*, H. Kieffer *et al.*, Eds. (Univ. of Arizona Press, Tucson, AZ, 1992), chap. 27.
49. J. E. Tillman, N. C. Johnson, P. Gettorp, D. B. Percival, *J. Geophys. Res.* **98**, 10963 (1993).
50. We acknowledge the extensive effort done by James Bell III and Timothy McConnochie in order to achieve relative calibration of THEMIS VIS images, including V00910003.

14 November 2002; accepted 25 November 2002
Published online 5 December 2002;
<zdoi;10.1126/science.1080497>
Include this information when citing this paper.

Fig. 1. Simultaneous THEMIS IR and VIS images near the south polar cap at L_s = 334°, illumination from the top. The false-color image is THEMIS IR image I00910002 (Band 9, 12.6 µm). The darkest areas in the image are near 145 K, and the brightest near 220 K; the strip is 32 km wide. The gray insert is THEMIS VIS image V00910003 (Band 3, 654 nm). The thermal image is overlaid with a sketch of the individual thermal units: C – Solid CO_2 on the surface; D – a dry gently sloping unit that is dark and hot (the classic "dark lanes" through the perennial cap); I – the flat-lying unit of intermediate albedo and temperature (water ice); and S – a warmer and darker flat-lying unit (soil). The numbered black rectangles are Regions of Interest (ROIs) used to accumulate seasonal data. The white rectangle outlines the position of the VIS image, shown to the right as the gray-scale image.

Fig. 2. TES thermal bolometer brightness temperatures vs. season for several units defined by small ROIs, and computed surface temperatures. In each case temperatures for unit C (CO_2) are shown in blue; their variation and trend are probably due largely to changing amounts of dust in the atmosphere. (**A**) ROI 1 in unit I. The open triangles are afternoon temperatures (16H) and the closed boxes are nighttime temperatures (23H). The red, orange, blue curves are thermal models for thermal inertia (TI) = 800, 1600, and 2000 [SI units], respectively. The solid curves are for 16H and the dashed curves are for 23H. (**B**) ROI 2 in unit S: Early seasonal trends are consistent with the high thermal inertia. The lines and symbols are the same as in Fig. 2A. (**C**) ROI 2 temperatures compared with two-layer thermal models. The symbols are the same as in Fig. 2A. The colored lines, red and blue, are for models with a thin layer and a medium layer of TI = 50 on top of TI = 2000, respectively. Late seasonal trends are bracketed by the models of thin (2 mm) to medium (7 mm) thickness surficial layer of I~50 covering a slab of H_2O ice.

Fig. 3. Visual MOC and Viking images showing the water ice unit near the south pole of Mars. (**A**) MOC Image M12-02286 (L_s = 306) shows unit I is largely covered by CO_2 ice. The "S' unit is exposed. (**B**) MOC image M14-00172 (Ls = 329) shows both units I and S exposed; unit I is visibly brighter than unit S. (**C**) A Viking visual image of the same region as the THEMIS IR image acquired 25 years ago (L_s = 348); unit I has intermediate brightness. (**D**) A sketch of the individual units on THEMIS thermal image: C – Solid CO_2 on the surface, D – a dry gently sloping unit that is dark and hot, I – the unit of intermediate albedo and temperature, and S – a warm dark unit.

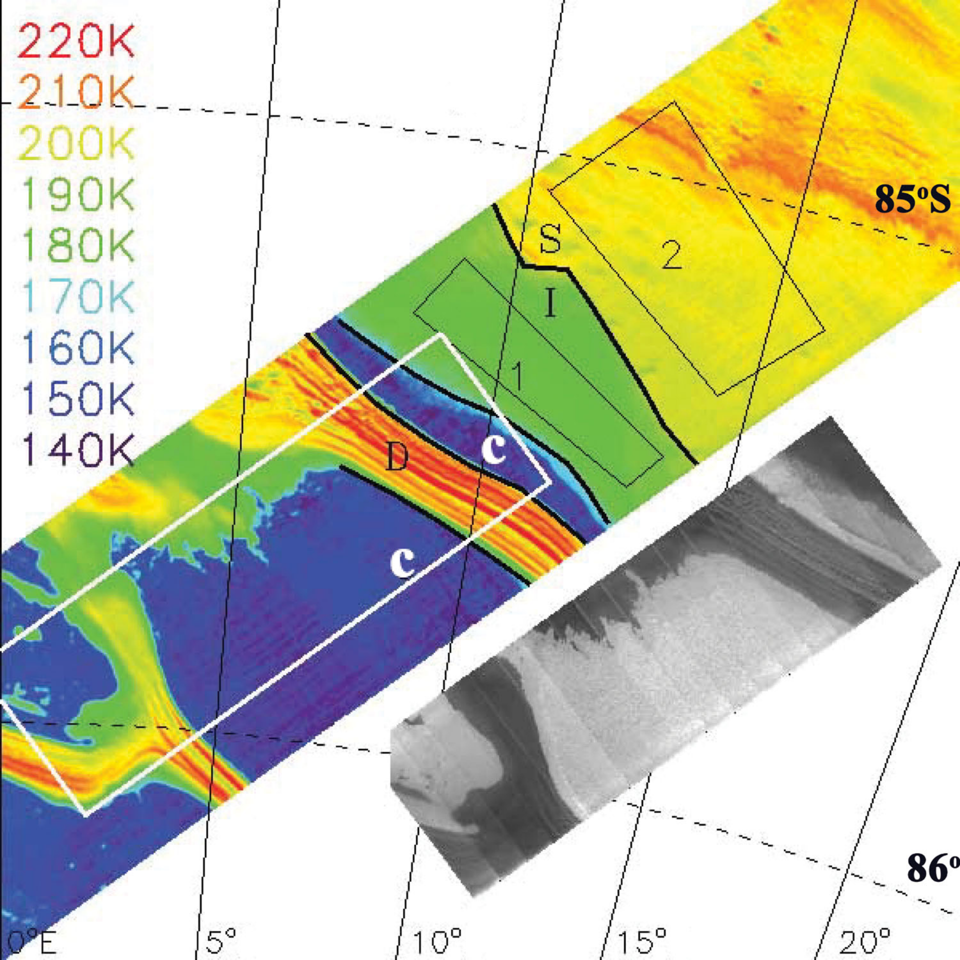
220K
210K
200K
190K
180K
170K
160K
150K
140K
85°S
86°
S
I
2
1
D
c
c
0°E
5°
10°
15°
20°

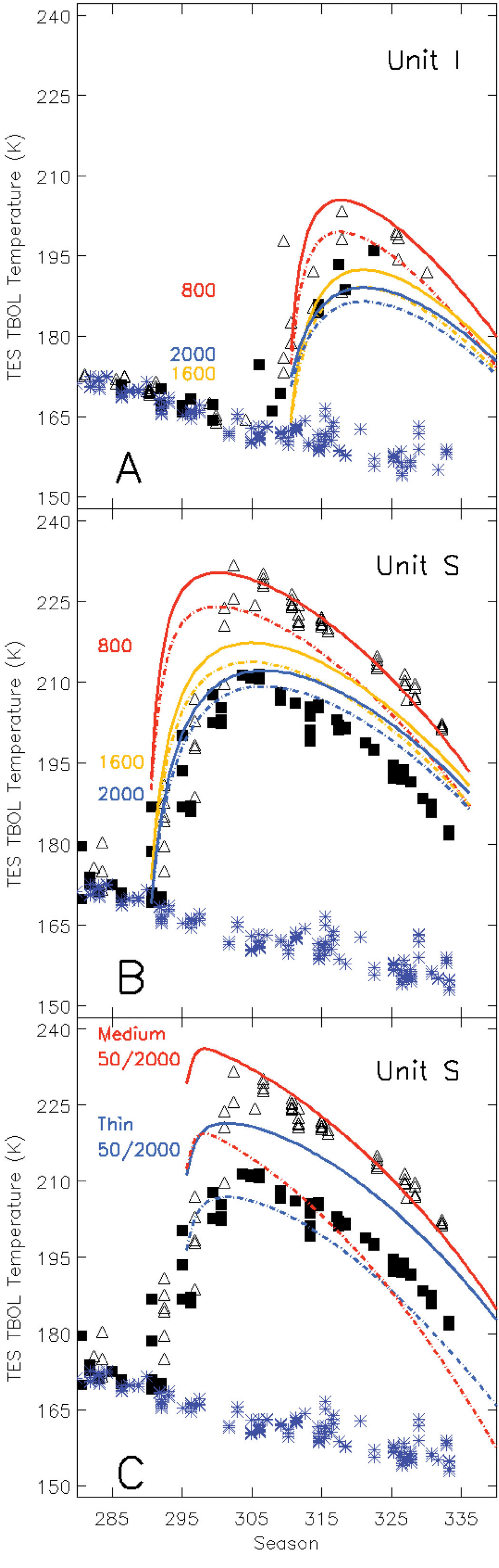
Unit I
800
2000
1600
A
Unit S
800
1600
2000
B
Medium
50/2000
Unit S
Thin
50/2000
C
TES TBOL Temperature (K)
240
225
210
195
180
165
150
285
295
305
315
325
335
Season

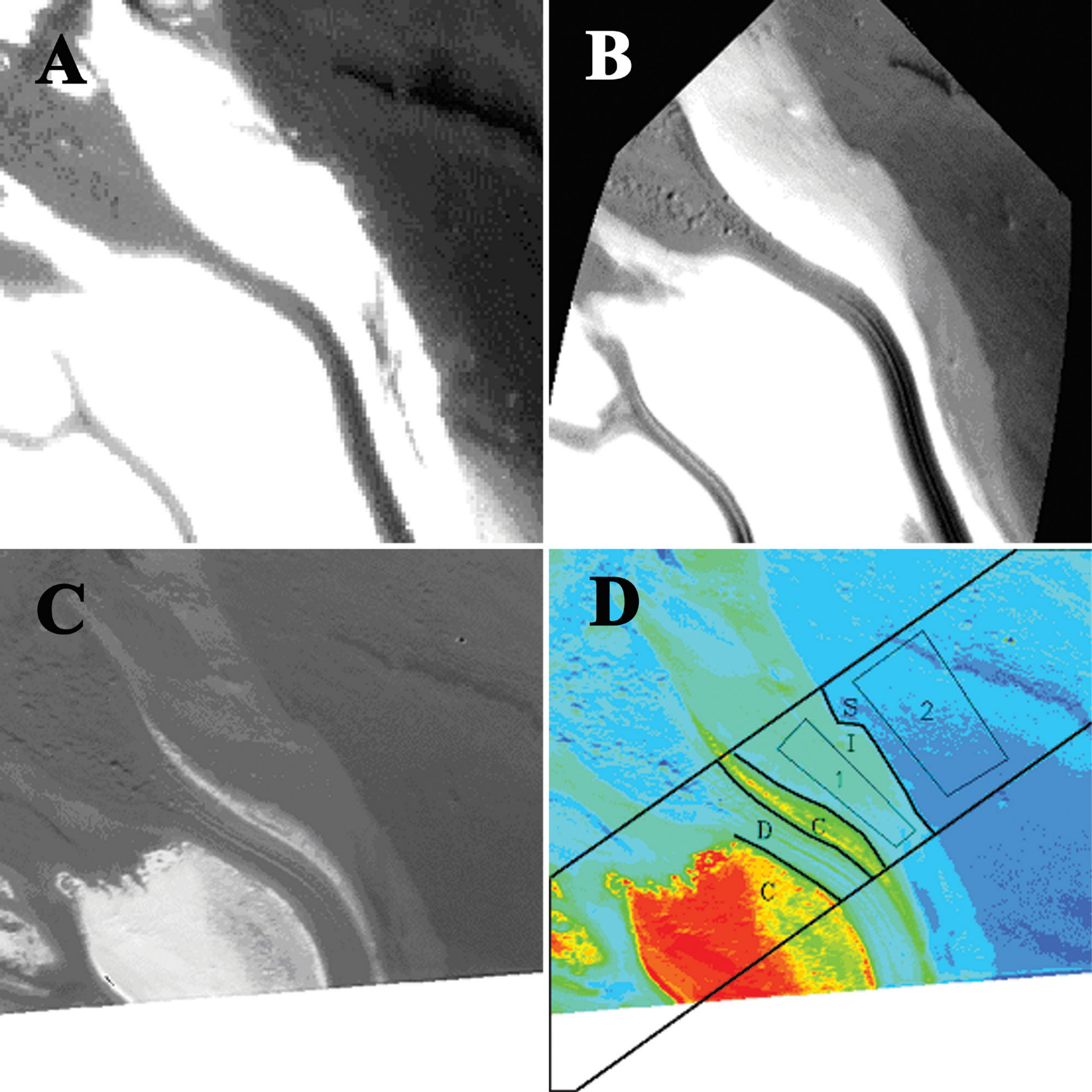
A
B
C
D
S
2
I
1
D
C
C